Simulation and characterization of cation disorder in $ZnGeP_2$

Jacob J. Cordell[a†]

National Renewable Energy Laboratory,

15027 Denver W Pkwy, Golden, CO 80401 and

Colorado School of Mines, 1500 Illinois St, Golden, CO 80401

Linda Pucurimay

National Renewable Energy Laboratory,

15027 Denver W Pkwy, Golden, CO 80401 and

Princeton University, Princeton, NJ 08544

Rekha R. Schnepf

National Renewable Energy Laboratory,

15027 Denver W Pkwy, Golden, CO 80401 and

Colorado School of Mines, 1500 Illinois St, Golden, CO 80401

Ben L. Levy-Wendt

SLAC National Accelerator Laboratory,

2575 Sand Hill Rd, Menlo Park, CA 94025 and

Stanford University, 450 Serra Mall, Stanford, CA 94305

Michael F. Toney

SLAC National Accelerator Laboratory,

2575 Sand Hill Rd, Menlo Park, CA 94025 and

Department of Chemical and Biological Engineering,

University of Colorado, Boulder, CO 80309

Garritt J. Tucker

Colorado School of Mines, 1500 Illinois St, Golden, CO 80401

Stephan Lany

[a] JC and LP contributed equally to this article

National Renewable Energy Laboratory,
15027 Denver W Pkwy, Golden, CO 80401

Adele C. Tamboli[‡]
National Renewable Energy Laboratory,
15027 Denver W Pkwy, Golden, CO 80401

(Dated: May 9, 2022)

Abstract

New optoelectronic materials are needed for improving the efficiency and reliability of devices such as solar cells. Cation ordering presents one means of controlling optoelectronic properties while introducing potential to also diversify the mineral constituents of electronic devices; however, the mechanisms of ordering are not yet well understood. To better understand cation ordering in a system integratable with current devices, we assess short- and long-range order parameters of $ZnGeP_2$, a material closely lattice-matched to Si. Structures are simulated using cluster-based Monte Carlo and first principles calculations to compare structural distortions, periodicity and local coordination environments in $ZnGeP_2$ to experimental data both from the literature and presented here. Comparing order parameters, we relate the transition in order parameters of $ZnGeP_2$ to that of $ZnGeN_2$, discuss the reduction of band gaps with disorder and show that traditional structural characterization alone is insufficient for understanding order in $ZnGeP_2$.

Keywords: phosphide, tunable, simulation, photovoltaic, semiconducting, computation

[†] Correspondence email address: cordell@mines.edu
[‡] Correspondence email address: atambolinrel@gmail.com

INTRODUCTION

$ZnGeP_2$ is a group II−IV−V_2 semiconductor that shows promise as a photovoltaic absorber. Its ternary character allows for the tuning of structural and optical properties at a specific composition by controlling cation site ordering, the swapping of atomic species on a fixed crystal lattice, without significant changes in the lattice constant. $ZnGeP_2$ has a predicted band gap of 2.1 eV in its ordered, ground state and is within 1% lattice matched to silicon.[1] Controlling the cation disorder in $ZnGeP_2$ could allow for tuning of the band gap to 1.7 eV, which would make it an ideal absorber material for a top cell in a Si-based tandem solar cell. [2] In this computationally-driven study, we develop a model to quantify site disorder in $ZnGeP_2$ and provide analysis of ordering in a set of $ZnGeP_2$ films to connect the understanding of theory and experiment.

Cation disorder has been studied in a variety of ternary and multinary materials due to its effect on electronic and optical properties.[3–11] It has been experimentally shown in bulk $ZnGeP_2$ that at equilibrium, $ZnGeP_2$ undergoes a solid state transformation at 950 °C from the ordered chalcopyrite phase to the disordered zinc-blende phase, where zinc and germanium will randomly occupy the cation sublattice.[12–14] It has been shown in both bulk [15, 16] and thin film [17] synthesis of $ZnGeP_2$ that processing conditions can be manipulated to grow varying degrees of disordered material below the transition temperature due to kinetic trapping. However, systematically controlling the degree of disorder in $ZnGeP_2$ films for its desired use as a photovoltaic material remains as an outstanding challenge due to the competition between high growth/anneal temperatures needed to achieve cation ordering and the volatility of Zn and P, which causes these ions to vaporize at high temperatures. [17, 18]

The experimental analysis and quantification of disorder in $ZnGeP_2$ is a challenge due to the similar atomic number (Z) of the Zn and Ge cations, [19] which requires a variable diffraction probe energy to deconvolve. This similarity causes Zn and Ge to be virtually indistinguishable in conventional X-ray Diffraction (XRD) and complicates the ability to determine the occupancy of the Zn and Ge sites. Using computationally simulated $ZnGeP_2$ structures with order parameters that have not yet been established experimentally, we aim to aid the characterization of ordering in $ZnGeP_2$, which is vital in the development of $ZnGeP_2$ as a novel material for optoelectronic devices.

To model cation disorder, we use cluster-based Monte Carlo (MC) to simulate $Zn_{Ge} + Ge_{Zn}$

pairs and relax resulting supercells using density functional theory with an applied Hubbard parameter to Zn (DFT+U). Previous studies of defects in $ZnGeP_2$ highlight these antisites as the most energetically favorable native defects [16, 20, 21]. While these antisites largely dictate the cation ordering of the system, the dominance of Zn_{Ge} and Ge_{Zn} does not preclude the existence of vacancies and interaction of native and extrinsic defects. [20] Ref. 21 for example shows through first principles calculations that P_{Ge} and Ge_P can also be relevant in addition to the cation-cation antisites under p-type and n-type conditions, respectively. This study focuses on the influence of stoichiometry-maintaining $Zn_{Ge} + Ge_{Zn}$ pairs on cation disorder, but we acknowledge the importance of other defects in the growth and optoelectronic utility of $ZnGeP_2$.

To measure site disorder computationally, Ref 22 reported that short-range order (SRO) and long-range order (LRO) parameters, rooted in shifts of free energy of the system, can be extracted from representative MC structures equilibrated as a function of effective temperature. SRO refers to the local arrangement of atoms.[23, 24] Here, SRO takes the form of the local cation coordination of P and the adherence of this environment to the octet rule, [25] which is only preserved in this system when P is coordinated by two Zn and two Ge. LRO refers to the global average occupancy of lattice sites and in this work indicates the similarity of a structure to the $ZnGeN_2$ ground state.[26, 27] The effective temperature in turn measures the thermodynamic temperature equivalent of a system at nonequilibrium. [22, 28] Applying this method to examine transitions in SRO and LRO in $ZnGeP_2$, we compare simulated and experimental order parameters to the literature on bulk [12–14, 29, 30] and film [17, 18, 31] syntheses to relate theory and experiment and better characterize cation disorder.

LOW ENERGY POLYTYPES

In the context of cation disorder, it is often instructive to consider low-energy, cation-ordered structures as a reference.[11] For example, Cu_2ZnSnS_4 (CZTS) has been found to exhibit different properties depending on the polymorphs present in a single phase. [32] Exploring the most thermodynamically favorable polytypes of a material allows us to search for and locate these structures in large supercells in a targeted manner. Through this identification process, it is then possible to see if a supercell contains multiple regions of different polytypes, i.e., if multiple low energy phases are present. In $ZnGeP_2$, the five lowest energy phases exhibit P coordinated

exclusively by two Zn and two Ge. This observation informs the search for short-range ordered, but long-range disordered (multiphase) supercells. Understanding the thermodynamics of polytypes of a material can also guide which signatures such as diffraction peaks and peak splitting we look for to identify the crystal structure in experimental characterization and differentiate between SRO and LRO.

In CZTS, ordering largely based on the kesterite $I\bar{4}$ (space group number 82), stannite $P\bar{4}2c$ (112) and $P\bar{4}2m$ (121) structures has been studied to determine stable polytypes. [33–35] These structures have a unit cell with a maximum of 16 atoms in their primitive cells, however, in $ZnGeP_2$, we find through investigating slightly larger cell sizes and relaxing these structures in DFT+U that two 32 atom unit cells also have energies close to the ground state chalcopyrite $I\bar{4}2d$ (122) structure. The zinc-blende-derived structure of $ZnGeP_2$, similar to that of CZTS, provides numerous polytypes with relatively small unit cells. Figure 1 shows the lowest energy structures of $ZnGeP_2$ as determined by relaxation using DFT+U and lists the structures' space group and formation enthalpy. c/a ratios listed in Figure 1 are normalized for comparison to the ground state conventional cell (structure A) so that shared cation occupancy on each cation site would yield $c/a = 2$ for each structure. The structures pictured in Figure 1 fall within 52 meV/cation of the ground state structure. The polytype search is not exhaustive, but includes structures with 8, 16 and 32 atoms with a variety of unit cell shapes represented. The two 32 atom structures lie lower in energy than structure D with a primitive cell composed of 16 atoms. Structure B can be constructed by stacking and alternately rotating conventional cells of structure A, whereas structure C constitutes stacking one of structure D with two of structure E. Alternatively, all of these structures can be made from the smallest stoichiometric building block, the primitive cell of structure E.

The polytypes shown in Figure 1 are the lowest energy polytypes found in this work and all of them are short-range ordered; each P is coordinated by exactly two Zn and two Ge. The fact that so many different SRO structures lie below non-SRO structures in energy emphasizes that octet-rule breaking coordination of P ions is thermodynamically unfavorable. Not shown among these polytypes is the zinc-blende-like phase with fully random cation occupation as this phase requires a larger cell or shared cation occupancies which cannot be simulated with available atomic potential files. The LRO parameter η quantifies the likeness of a structure to the ground state.

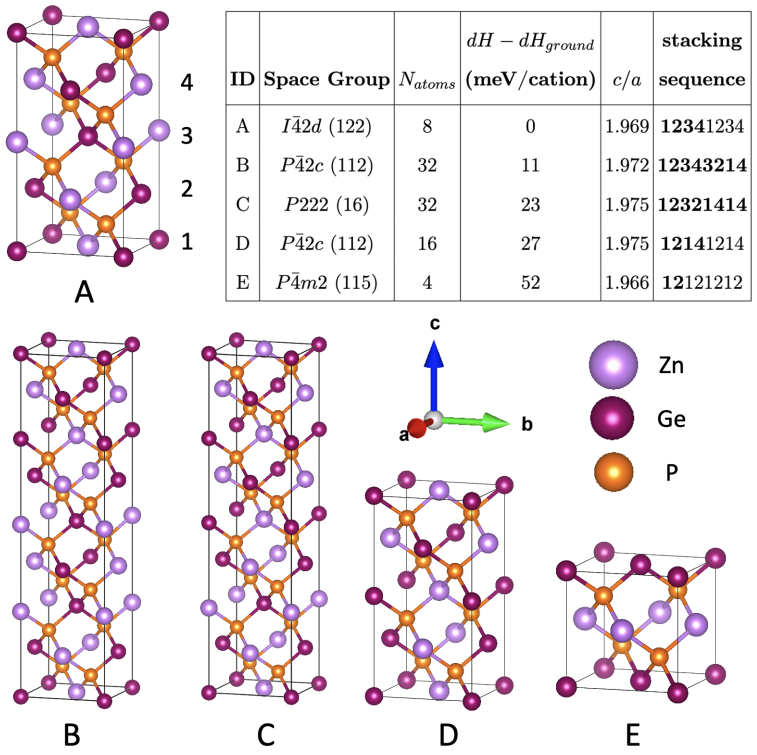

ID	Space Group	N_{atoms}	$dH - dH_{ground}$ (meV/cation)	c/a	stacking sequence
A	$I\bar{4}2d$ (122)	8	0	1.969	**12341234**
B	$P\bar{4}2c$ (112)	32	11	1.972	**12343214**
C	$P222$ (16)	32	23	1.975	**12321414**
D	$P\bar{4}2c$ (112)	16	27	1.975	**12141214**
E	$P\bar{4}m2$ (115)	4	52	1.966	**12**121212

Figure 1. Conventional cells of low energy polytypes of $ZnGeP_2$ along with their space groups, number of atoms in primitive cell, difference in formation enthalpy between each structure and the ground state of $ZnGeP_2$, c/a and stacking sequence distinguishing each polytype. Numbers to the right of Structure A indicate the stacking sequence of planes in the c direction.

$$\eta = r_\alpha + r_\beta - 1 \tag{1}$$

where r_α is the fraction of site α occupied by atom α. [26, 27] However, as sophisticated XRD characterization tools are often needed to accurately determine η, the c/a ratio is often used in its place in experiment.[36, 37] c/a changes with degree of ordering because ordering distorts structures and in $ZnGeP_2$ reduces the perceived symmetry away from the zinc-blende pattern detected with X-ray techniques when cation occupancies are fully random. The c/a ratios for structures A through E in Figure 1 are all similar to each other meaning that this parameter alone is not enough to distinguish between the set. c/a is easier to characterize than η, but few experimental studies are available to compare how c/a and η are related in $ZnGeP_2$. By modeling disordered $ZnGeP_2$ we are able to determine a more clear relationship between c/a and

η. In addition, we are able to determine the local ordering of these structures quantified as the fraction of phosphorus with each possible tetrahedral coordination motif, which we use as a SRO parameter.

In quantifying both the coordination of phosphorus and η, we can immediately identify the presence of polytypes in a sample. High fractions of phosphorus coordinated by two Zn and two Ge paired with a low η indicate the presence of non-ground state polytypes. Perfect SRO-type coordination and $\eta < 1$ would indicate a mixed phase of multiple polytypes creating perfect SRO, but long-range disorder. In $ZnGeP_2$, the larger difference in cation size drives LRO like in $ZnGeN_2$ [22], but unlike $ZnSnN_2$, which has more similar cation-anion bond lengths. [38] SRO in $ZnGeP_2$ in turn is driven by local conservation of the octet-rule. SRO presents different challenges than LRO to experimentally characterize and likewise controls many optical and electronic properties of the system.

SHORT-RANGE ORDER

The LRO parameter has been utilized as a metric for quantifying cation disorder in experimental studies of $ZnGeP_2$ [17] and in theoretical studies of $ZnGeN_2$ [22]. We use η along with the motif fraction of $P{-}Zn_2Ge_2$ or SRO parameter to identify the phase transition from ordered to disordered material as a function of effective temperature [28] through MC simulations between 1000K and 5000K. The effective temperature accounts for the kinetic limitations of non-equilibrium growth, such as chemical vapor deposition or sputtering. Experimental syntheses of $ZnGeP_2$ have demonstrated that the annealing temperature and the annealing time play significant roles in phase transitions. It has been reported that amorphous $ZnGeP_2$ films form a disordered crystalline phase upon annealing for an hour at 500°C.[17] Upon further annealing of the films at 700°C for an hour, the films transition to an energetically favorable ordered phase. This phenomenon is indicated by peak splitting in the {220} and {311} peaks in the XRD patterns. Bulk studies of $ZnGeP_2$ report that at 950°C, a transition from ordered phase to a disordered phase occurs.[14] However, quantifying the site disorder in $ZnGeP_2$ is a challenge due to the similar Z number between Zn and Ge.

We investigate the SRO transition by using the fraction of short-range motifs as a function of effective temperature in computationally generated supercells. The Zn_2Ge_2 motif conserves the

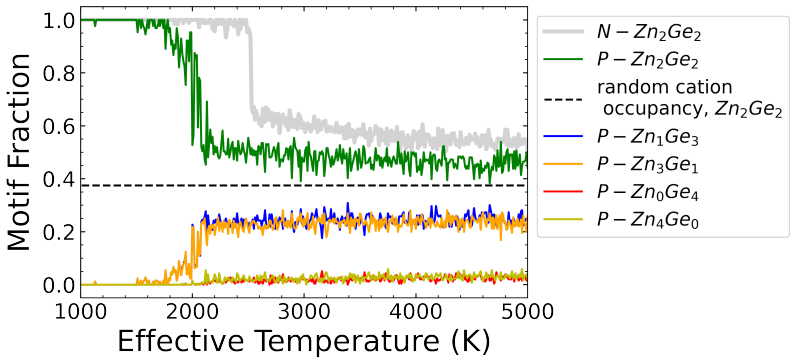

Figure 2. Fraction of anion-centered motifs for $ZnGeP_2$ as a function of simulated temperature with ordered (Zn_2Ge_2) displayed for $ZnGeN_2$ for reference.

octet rule locally. The fraction of this motif is defined as the ratio of all P anions coordinated by two Zn and two Ge cations, in contrast to the octet rule breaking counterparts (P−Zn_1Ge_3, P−Zn_0Ge_4, P−Zn_4Ge_0, P−Zn_3Ge_1), which indicate short-range disorder. Figure 2 shows these motif fractions for $ZnGeP_2$ as well as the Zn_2Ge_2 motif fraction of $ZnGeN_2$ as a function of effective temperature. We identify a change at 2000K from solely octet rule conserving motifs to a combination of motif types. In the nitride counterpart, $ZnGeN_2$, this transition occurs at a higher effective temperature of 2500K.[22] The sharp phase transition in $ZnGeN_2$ results in near-binary behavior of the material resulting in either almost fully ordered or already strongly disordered (but not fully random) structures. The less steep transition in $ZnGeP_2$ creates a wider range of order parameter values accessible in $ZnGeP_2$ than in $ZnGeN_2$. Further, we observe that the distribution of motifs comes closer to that for random cation occupancies at lower temperatures in $ZnGeP_2$ than in $ZnGeN_2$. Random cation occupancy yields a fraction of Zn_2Ge_2 of 0.375 as 6 of the 16 possible decorations of Zn and Ge are this motif. At 3000K, the fraction of Zn_2Ge_2 hovers close to 0.5 for the phosphide, well below the value of 0.6 for the nitride. This difference in ordering shows the greater accessibility of a wider range of SRO parameters in $ZnGeP_2$ than in $ZnGeN_2$.

LONG-RANGE ORDER

The more continuous transition from short-range ordered to disordered material in $ZnGeP_2$ compared to $ZnGeN_2$ provides a larger window of possible synthesis conditions for accessing intermediate order parameters. While Figure 2 shows the range of local motifs present, Figure 3 shows that LRO as defined in Equation 1 closely follows the trends of SRO represented as nitrogen coordination.

Because of the large number of polytypes of $ZnGeP_2$ close in energy to the ground state, one may expect to see short-range ordered structures that break LRO due to irregular stacking sequences of the different polytypes. Investigating the stacking of multiple SRO structures is rendered possible by simulating disorder in cells with several hundred atoms. Similar SRO structures have been observed in computational studies of $ZnSnN_2$ [39, 40]. However, cells with a high degree of SRO and low degree of LRO are not observed in Figure 3. In contrast, LRO trends strongly and linearly with SRO for values of each close to one, while the trend is less strong, but similarly linear for SRO and LRO parameters below 0.7. The strong correlation between SRO and LRO precludes the possibility of a short-range ordered, but long-range disordered phase such as that described in $(ZnSnN_2)_{0.75}(ZnO)_{0.5}$.[38] In $(ZnSnN_2)_{0.75}(ZnO)_{0.5}$, short-range disorder creates localized states that are mitigated in the perfect SRO, but long-range disordered phase. However, in $ZnGeP_2$, states are not as prone to localize with site disorder as in its similar nitride counterparts, which we describe in further detail below. The less localized states of $ZnGeP_2$ mean that the SRO phase comprised of a mix of polytypes is not needed as in $(ZnSnN_2)_{0.75}(ZnO)_{0.5}$ to obtain reasonably efficient carrier transport.

The LRO parameter η can be determined from diffraction [41] using Rietveld refinement to obtain the occupancies of cation sites [42, 43], however, the similar scattering factors of Zn and Ge can make these occupancies difficult to determine. The ratio of c/a is also commonly used as a proxy for LRO [17, 30, 44, 45]. The c/a ratio provides an estimate of the LRO parameter by showing the distortion of $ZnGeP_2$ between its ordered tetragonal form and its disordered cubic form ($c/a \equiv 2$), for fully random cation occupations. Experimental techniques [12–14, 17, 29, 30, 46, 47] yield values of c/a between 1.96 and 1.97, with 1.969 calculated for the relaxed unit cell here (1.968 using a more accurate SCAN functional [48, 49]). In computations, the local density approximation (LDA) results in lower c/a [50] and the generalized gradient approximation (GGA),

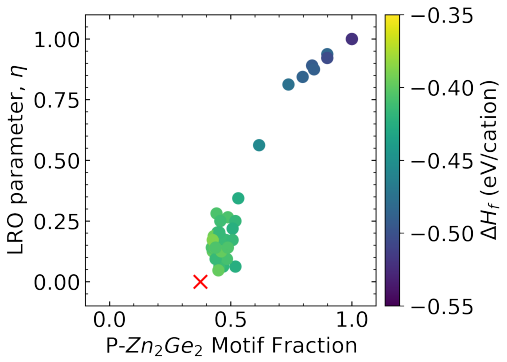

Figure 3. Comparison of SRO and LRO in simulated $ZnGeP_2$ cells. The × indicates the parameters for a random configuration of cations ($\eta = 0$, P−Zn_2Ge_2= 0.375).

higher assessments of c/a [51] although all are within the experimental range. [52] Differences in values among experiments could be due in part to the specific stoichiometries of each bulk sample or film measured. As an example of stoichiometry impacting c/a, Zn and P vacancies disproportionately relax c more so than a where the material is at least partially ordered. In the 16 atom conventional ordered cell (structure A, Figure 1), a single V_P reduces c/a from 1.969 to 1.951 and V_{Zn} to 1.941, both independent of which P or Zn site is chosen. The reductions in c/a would be much less pronounced for a smaller concentration of vacancies, but nonetheless, stoichiometry plays a significant role in determining the structural distortions that control c/a.

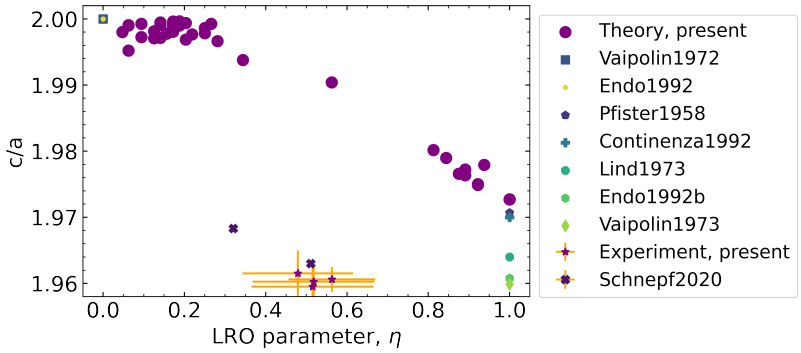

Figure 4. c/a ratios calculated from combinatorial $ZnGeP_2$ films using Rietveld refinements and computationally relaxed structures from MC simulation plotted against LRO parameter. Experimental data from the available literature are shown for reference.[17, 29, 53–58]

Figure 4 shows the mapping between c/a and η for data from MC simulations at effective temperatures between 1000K and 5000K. Experimental samples, deposited using combinatorial sputtering provide a reference for $\eta \approx 0.5$. Films from both the present study and Ref. 17 were amorphous as-deposited and only crystallized with the order parameters shown in Figure 4 after annealing. The error bars in the LRO parameters for the samples added here are larger than the previously reported data due to using only two diffraction energies in the refinement. The data reported in Ref. 17 uses resonant energy X-ray diffraction (REXD) data for the individual superlattice peak over a range of energies surrounding the Zn and Ge absorption edges, which adds more certainty in the extracted occupancies. Data from Ref. 29, 53–58 were taken from the Inorganic Crystal Structure Database (ICSD) [59] for refinements of experimental structures assuming either a perfectly disordered (zinc-blende) or ground state (chalcopyrite) structure. Measurement uncertainties are not available for these publications where the evaluations of c/a can be seen to span a wide range where η is assumed to be 1 for the purpose of refining diffraction data to obtain lattice parameters. Whereas the computational data indicates an almost linear correlation between η and c/a, the experimental data suggests even a strong reduction of η to 0.5 would not lead to a noticeable change in c/a making c/a an incomplete and potentially misleading depiction of ordering in $ZnGeP_2$.

Obtaining η from diffraction requires more information than c/a (i.e., REXD or a variable energy probe particle as opposed to conventional XRD). While both parameters are sensitive to structural distortions in the material from a variety of environmental factors, the sensitivity of c/a and η to these different factors such as stoichiometry and strain environment remains unclear. We show that a relationship can be established between the two parameters when stoichiometry is fixed and conditions are ideal. However, due to the intricacies of material growth c/a should not be used to infer order parameter alone.

A. Influence of disorder on band gap

Now that we have discussed how site order is quantified in $ZnGeP_2$, we can examine the role disorder plays on some of the material's properties. Specifically, the band gap of ordered $ZnGeP_2$ has been observed at around 2.2 eV through measuring the material's absorption onset [13] and decreases when disordered [17, 20]. Figure 5 displays band gaps from DFT+U with GW

corrections applied as a constant offset to the band edges. The band gaps are plotted as a function of order parameter along with absorption onset energies from selected experimental studies. The GGA+U calculations used in this work underestimate band gaps by around 1 eV in this system so GW corrections are used to recover more accurate valence and conduction band edge energies as described in the Methods Section. The calculated band gaps can be seen to decrease readily with LRO in mostly ordered structures before tapering to a more constant 0.98 ± 0.12 eV for $\eta < 0.5$. The ideal band gap of $ZnGeP_2$ targeted for a top cell absorber on Si photovoltaics of 1.7 eV [60] can be obtained with an order parameter of around $\eta = 0.9$ according to Figure 5.

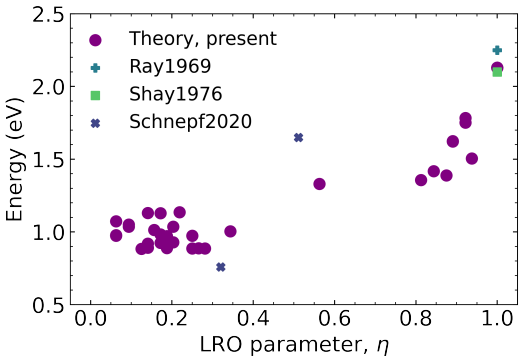

Figure 5. Band gaps from GW-corrected DFT+U and absorption onsets from experimental literature for $ZnGeP_2$ as a function of LRO.[13, 17, 61]

In $ZnGeN_2$, it was discovered that decreasing LRO similarly reduces the band gap of the system; however there are notable differences in the development of the band structure and carrier localization with ordering between $ZnGeN_2$ and $ZnGeP_2$.[62] These differences can be seen first in the trend in band gap, which stays present even for near-random cation configurations in $ZnGeP_2$ compared to in $ZnGeN_2$, where the gap closes to a metallic state in the random limit of disorder. In $ZnGeN_2$, this band gap narrowing also pairs with localized states that form deep in the gap. Highly localized states can act as traps decreasing the internal quantum efficiency of a photovoltaic device. Localized states can be tracked in computationally generated cells through the Inverse Participation Ratio (IPR). $\mathrm{IPR}(E) = \frac{N_A \sum_i p_i(E)^2}{[\sum_i p_i(E)]^2}$, where N_A is the number of atoms in a supercell and $p_i(E)$ is the local density of states (LDOS) projected on atom i as a function of energy E. An IPR of 1 indicates an ideal, charge-delocalized situation, while the higher the IPR (with a maximum of the number of atoms in the supercell), the more localized a state.

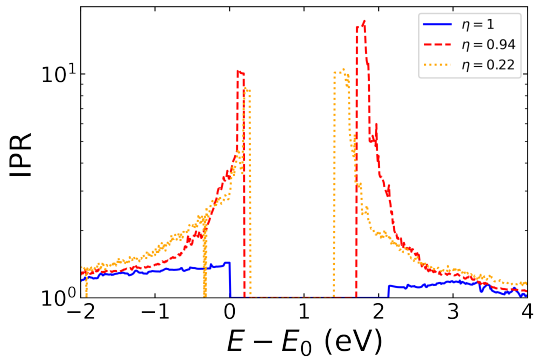

Figure 6. Inverse Participation Ratio of representative $ZnGeP_2$ supercells. $E - E_0$ is set to zero at the valence band maximum of the ordered $ZnGeP_2$ structure.

In $ZnGeN_2$, these localized states exceed an IPR of 200 in 1024 atom supercells[62] and in $(ZnSnN_2)_{0.75}(ZnO)_{0.5}$ can exceed values of 30 in 128 atom supercells[38]. The IPR near band edges in disordered $ZnGeP_2$ remains below 25 in 512 atom supercells indicating a much lower degree of carrier localization as displayed in Figure 6 for representative structures. Conduction band states also play a larger role in the IPR of $ZnGeP_2$ than in $ZnSnN_2$, where localization is largely seen in valence band states. $ZnGeP_2$ structures represented in Figure 5 additionally do not form any deep gap states as in the case of $ZnGeN_2$. The reduction in band gap with disorder in $ZnGeP_2$ paired with a lack of deep gap states and highly localized carriers remains promising for using disordered $ZnGeP_2$ in optoelectronic applications.

CONCLUSION

Simulating $ZnGeP_2$, we assess the relationship between structural deformation and cation order. Site disorder remains difficult to characterize as variable energy sources are often needed to gain in-depth understanding of a system's local and long-range order. Structural distortions which impact lattice parameters do not fully capture the ordering of a system because conducting refinements to determine lattice parameters requires first making assumptions about the order of a given system. The distinction of ordering is made trickier in $ZnGeP_2$ than in $ZnGeN_2$ because the smooth transition from SRO to disorder in $ZnGeP_2$ allows for the synthesis of nearly any degree of ordering under the right conditions. In contrast, the steep transition of $ZnGeN_2$

ensures that only mostly ordered or mostly disordered (and not intermediate values of η) can be reasonably expected in crystal syntheses making characterization nearly binary between the two possible states. Additionally, the conditions for creating fully random cation occupancies are more accessible in the phosphide than the nitride because simulations indicate zinc-blende-like structures can be achieved at significantly lower effective temperatures in $ZnGeP_2$ than wurtzite in $ZnGeN_2$ if the kinetics of the systems are otherwise comparable.

The band gap of $ZnGeP_2$ decreases with decreasing LRO and could be targeted to the desired 1.7 eV for tandem photovoltaics with Si at an order parameter of roughly $\eta = 0.9$. Unlike similar semiconducting materials, this decrease in band gap occurs without a high probability of localized carriers and deep-gap defect states, which can often be detrimental to the performance of optoelectronic devices. Understanding the transitions between order and disorder in ternary systems is necessary for controlling synthesis to capture the benefits of mixed ion semiconductors, many of which are sought for the earth abundance of their constituent elements and potential for their reduced climate impact compared to processing of current commercial materials. To characterize the order of $ZnGeP_2$ and similar systems, more direct probing of short- and long-range order is needed in addition to determining the overall structure of each sample of material.

METHODS

First Principles Calculations

Formation energies and lattice parameters for determining c/a ratios were calculated using DFT+U. The volume, shape and positions of ion configurations were relaxed from cells containing 512 atoms equilibrated through MC simulations. We used the Perdew-Burke-Ernzerhof (PBE) variety of the generalized gradient approximation (GGA) [63] for relaxations implemented in the Vienna Ab-initio Simulation Package (VASP) with a 2x2x2 Gamma-centered k-mesh. Formation enthalpies were determined by referencing energies from DFT+U to Fitted Elemental Reference Energies (FERE) from Ref. 64: -0.5 eV for Zn, -4.14 eV for Ge and -5.64 eV for P. In compliance with the methods for determining the FERE, Kresse-Joubert projector augmented wave datasets were used with pseudopotentials from VASP version 4.6 (Ge_d, P and Zn) and an energy cutoff of 380 eV. [65] Energy and force convergence criteria for ionic relaxation were set to 10^{-5} eV and

0.02 eV $Å^{-1}$, respectively on each atom. A Coulomb potential of $U - J = 6$ eV was applied to the Zn d orbital following the Dudarev approach [66].

Relaxations of polytypes shown in Figure 1 used the same calculation parameters listed above, but as unit cells only contained the number of atoms of each primitive cell, more k-points were needed. An 8x8x8 k-point grid was used for the primitive cell of structure A, and an equivalent density k-mesh was used for each other polytype. Band gaps and IPR calculations were obtained by post-processing of the self-consistent step following ion relaxation. GW corrections to the VBM and CBM were applied to reproduce the ordered band gap from GW calculations using correction factors from the National Renewable Energy Laboratory Materials Database (NRELMatDB).[67, 68]

Monte Carlo Simulations

Using MC simulations for 512 atom cells of $ZnGeP_2$, we investigate the cation ordering and formation enthalpy as a function of effective temperature. We use the clusters approach to statistical mechanics (CASM) software [69, 70] to set up a Hamiltonian for comparing structures in our MC simulations and use first-principles calculations to generate a set of energetically representative structures for $ZnGeP_2$ with varying degrees of cation order. Using a cluster expansion to model formation enthalpy captures both SRO and LRO. The cluster expansion has the form

$$H = \sum_{\alpha} m_{\alpha} J_{\alpha} \langle \prod_{i \in \beta} \sigma_i \rangle \tag{2}$$

where H is the enthalpy of formation, m is the multiplicity and J corresponds to the energy parameter of each cluster α. σ_i corresponds to the occupation on the lattice site, β represents the clusters symmetrically equivalent to α and i is the index of the atoms in a cluster β.

We generate a training set for the cluster expansion from DFT+U calculations. The atomic structures for $ZnGeP_2$ were generated from a primitive ideal zinc-blende cell with phosphorus as the anion and a generic cation site. The training and test structures were selected from a set of 47 structures, made up of 36 16-atom supercells, 9 8-atom supercells, and 2 4-atom supercells. We partitioned these structures into 3 sets of training and testing sets, where the training sets contained about 80% of the structures and the testing set was comprised of the remaining 20% of the structures. The selected training set for this computational study included all 9 8-atom

supercells, 2 4-atom supercells and 26 16-atom supercells and the ground state SG122 structure was specifically included. We calculate the total energies of the training and test structures using DFT+U and performed structural relaxations. The formation enthalpy of the SG122 ground state structure is calculated to be -521 meV/cat. Supercell sizes between 4 and 32 atoms were used for cluster expansion fitting. For the MC simulations, we generated 128 atom, 512 atom, and 1024 atom cells.

Experimental $ZnGeP_2$ Growth and Characterization

$ZnGeP_2$ thin films were grown using combinatorial reactive sputtering with PH_3 gas. Details on this method and the necessary safety precautions for handling PH_3 are described in Ref. 18. The films were grown at low temperatures to maintain Zn and P content. As a result, the films were amorphous as deposited. To crystallize the films, they were annealed ex-situ at 700°C for either 1 or 2 hours in ampoules with N_2 or Ar_2 gas.

Film composition was determined using X-ray Fluorescence (XRF) with a Bruker M4 Tornado Micro-XRF spectrometer, using a Rh excitation beam and two detectors. The XRF spectra was then modeled to extract the film composition using the XMethods software package. The XRF model utilized had previously been calibrated with Rutherford backscattering (RBS) data.

To obtain structural information such as c/a and LRO, we performed high-resolution XRD on and off the Zn absorption edge at the Stanford Synchrotron Radiation Lightsource (SSRL) beamline 2-1. Measuring at the Zn edge allows us to see super lattice peaks in samples with cation ordering. The incident angle was fixed at 3°and a Pilatus 100K detector was used. Full pattern scans were conducted over a large Q range with incident energies at the Zinc K-edge (9,659 eV) and at an off-resonant energy (10,500 eV). Rietveld refinements were then performed on REXD data using the TOPAS 6 Academic software package with a similar procedure to the one described in Ref. 17. First, the off-resonant full pattern was fit to extract lattice parameters, the phosphorus atomic position, the thermal parameter, and texturing. The chalcopyrite structure, $I\bar{4}2d$, was used as the base structure for the refinement. The occupancy values were then determined by simultaneously refining the off-resonant and Zn K-edge full pattern scans. The Zn and Ge cation sites (Wyckoff positions 2a and 2b) were allowed to be occupied by either Zn or Ge. The total occupancy on each site was constrained such that it could not exceed one. Quadratic penalties

were used to constrain the overall composition to that determined by XRF. Error bars were determined in TOPAS based on the quality of the refinement fit.

MONTE CARLO SIZE CONVERGENCE

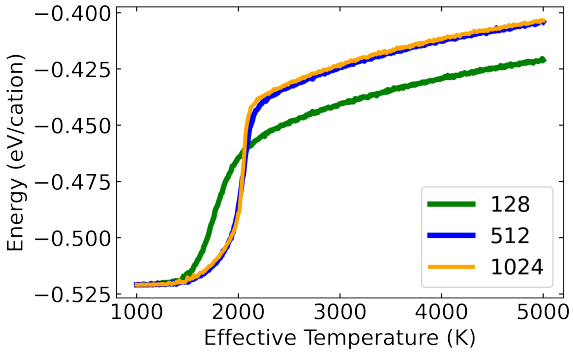

Figure 7. Comparison of MC simulations performed with varied cell size. The legend indicates the number of atoms in each cell.

MC simulations and subsequent relaxations in DFT+U used 512 atom cells. The supercell size was chosen as a compromise between reducing the computational cost of DFT+U calculations and minimizing finite size effects that would otherwise control order parameters. Figure 7 compares MC simulations of $ZnGeP_2$ using cells with 128, 512 and 1024 atoms with shapes of 2x2x2, 4x4x2 and 4x4x4 of the conventional 16 atom cell, structure A in Figure 1. Figure 7 shows that too small a cell size results in a smoothed out transition occurring at a lower effective temperature and with lower energy than predicted by larger cells. 512 atoms sufficiently mitigates self interaction of atoms across periodic boundaries and closely matches the formation enthalpy predicted for larger cells as a function of temperature.

DECLARATIONS

Funding

Primary funding was provided by the US. Department of Energy, Office of Science, Basic Energy Sciences, Materials Sciences and Engineering Division. The Alliance for Sustainable Energy,

LLC, operates and manages the National Renewable Energy Laboratory for the US. Department of Energy (DOE) under Contract No. DE-AC36-08GO28308. L. P. thanks DOE Office of Science under the Science Undergraduate Laboratory Internship Program (SULI) for financial support in 2021. R. R. S. acknowledges support from the National Science Foundation Graduate Research Fellowship under Grant No. 1646713. The research was performed using computational resources sponsored by the Department of Energy's Office of Energy Efficiency and Renewable Energy and located at the NREL. B.L.L.-W and M.F.T acknowledge support from the National Science Foundation, DMREF No. 1729594. The views expressed in the article do not necessarily represent the views of the DOE or the US. Government. The U.S. Government retains and the publisher, by accepting the article for publication, acknowledges that the U.S. Government retains a nonexclusive, paid-up, irrevocable, worldwide license to publish or reproduce the published form of this work, or allow others to do so, for U.S. Government purposes.

Conflicts of interest/Competing interests

The authors declare no conflict of interest.

Availability of data and code

Structure files used in this work are provided in the Supplemental Information along with representative Rietveld refinement data. Additional data and code are available upon reasonable request.

Authors' contributions

JC: investigation, conceptualization, methodology, software, formal analysis, writing, editing, visualization, resources LP: investigation, software, validation, formal analysis, writing, editing, funding acquisition RS: investigation, writing, editing BLW: investigation, editing GT: resources, editing, supervision MT: resources, supervision SL: investigation, conceptualization, resources

AT: conceptualization, resources, editing, funding acquisition, supervision

---

[1] Aaron D Martinez, Angela N Fioretti, Eric S Toberer, and Adele C Tamboli. Synthesis, structure, and optoelectronic properties of II−IV−V2 materials. *Journal of Materials Chemistry A*, 5(23):11418–11435, 2017.

[2] Rekha R Schnepf, Aaron D Martinez, John S Mangum, Laura T Schelhas, Eric S Toberer, and Adele C Tamboli. Disorder-tunable $ZnGeP_2$ for epitaxial top cells on Si. In *2019 IEEE 46th Photovoltaic Specialists Conference (PVSC)*, pages 1052–1055. IEEE, 2019.

[3] Wenhao Sun, Christopher J Bartel, Elisabetta Arca, Sage R Bauers, Bethany Matthews, Bernardo Orvañanos, Bor-Rong Chen, Michael F Toney, Laura T Schelhas, William Tumas, et al. A map of the inorganic ternary metal nitrides. *Nature materials*, 18(7):732, 2019.

[4] Yoyo Hinuma, Taisuke Hatakeyama, Yu Kumagai, Lee A Burton, Hikaru Sato, Yoshinori Muraba, Soshi Iimura, Hidenori Hiramatsu, Isao Tanaka, Hideo Hosono, et al. Discovery of earth-abundant nitride semiconductors by computational screening and high-pressure synthesis. *Nature communications*, 7(1):1–10, 2016.

[5] Theresa M Christian, Daniel A Beaton, Kunal Mukherjee, Kirstin Alberi, Eugene A Fitzgerald, and Angelo Mascarenhas. Amber-green light-emitting diodes using order-disorder $Al_xIn_{1-x}P$ heterostructures. *Journal of Applied Physics*, 114(7):074505, 2013.

[6] Eric W Blanton, Keliang He, Jie Shan, and Kathleen Kash. Characterization and control of $ZnGeN_2$ cation lattice ordering. *Journal of Crystal Growth*, 461:38–45, 2017.

[7] Elisabetta Arca, John D Perkins, Stephan Lany, Allison Mis, Bor-Rong Chen, Patricia Dippo, Jonathan L Partridge, Wenhao Sun, Aaron Holder, Adele C Tamboli, et al. Zn_2SbN_3: Growth and characterization of a metastable photoactive semiconductor. *Materials Horizons*, 6(8):1669–1674, 2019.

[8] Robert A Makin, Krystal York, Steven M Durbin, Nancy Senabulya, James Mathis, Roy Clarke, Nathaniel Feldberg, Patrice Miska, Christina M Jones, Zihao Deng, et al. Alloy-free band gap tuning across the visible spectrum. *Physical Review Letters*, 122(25):256403, 2019.

[9] Celeste L Melamed, Jie Pan, Allison Mis, Karen Heinselman, Rekha R Schnepf, Rachel Woods-Robinson, Jacob J Cordell, Stephan Lany, Eric S Toberer, and Adele C Tamboli. Combinatorial

investigation of structural and optical properties of cation-disordered zngen 2. *Journal of Materials Chemistry C*, 8(26):8736–8746, 2020.

[10] Ann L Greenaway, Amanda L Loutris, Karen N Heinselman, Celeste L Melamed, Rekha R Schnepf, M Brooks Tellekamp, Rachel Woods-Robinson, Rachel Sherbondy, Dylan Bardgett, Sage Bauers, et al. Combinatorial synthesis of magnesium tin nitride semiconductors. *Journal of the American Chemical Society*, 142(18):8421–8430, 2020.

[11] Allison Mis, Stephan Lany, Geoff L Brennecka, and Adele Tamboli. Exploring the phase space of Zn_2SbN_3, a novel semiconducting nitride. *Journal of Materials Chemistry C*, 9(39):13904–13913, 2021.

[12] K Masumoto, S Isomura, and W Goto. The preparation and properties of $ZnSiAs_2$, $ZnGeP_2$ and $CdGeP_2$ semiconducting compounds. *Journal of Physics and Chemistry of Solids*, 27(11-12):1939–1947, 1966.

[13] B Ray, AJ Payne, and GJ Burrell. Preparation and some physical properties of $ZnGeP_2$. *physica status solidi (b)*, 35(1):197–204, 1969.

[14] E Buehler, JH Wernick, and JD Wiley. The ZnP_2−Ge system and growth of single crystals of $ZnGeP_2$. *Journal of Electronic Materials*, 2(3):445–454, 1973.

[15] Y Shimony, G Kimmel, O Raz, and MP Dariel. X-ray diffraction analysis of melt-grown $ZnGeP_2$(ZGP). *Journal of crystal growth*, 198:583–587, 1999.

[16] Y Shimony, O Raz, G Kimmel, and MP Dariel. On defects in tetragonal $ZnGeP_2$ crystals. *Optical Materials*, 13(1):101–109, 1999.

[17] Rekha R Schnepf, Ben L Levy-Wendt, M Brooks Tellekamp, Brenden R Ortiz, Celeste L Melamed, Laura T Schelhas, Kevin H Stone, Michael F Toney, Eric S Toberer, and Adele C Tamboli. Using resonant energy x-ray diffraction to extract chemical order parameters in ternary semiconductors. *Journal of Materials Chemistry C*, 8(13):4350–4356, 2020.

[18] Rekha R Schnepf, Andrea Crovetto, Prashun Gorai, Anna Park, Megan Holtz, Karen N Heiselman, Sage R Bauers, Brooks M Tellekamp, Andriy Zakutayev, Ann L Greenaway, Eric S Toberer, and Adele C Tamboli. Reactive phosphine combinatorial co-sputtering of cation disordered $ZnGeP_2$ films. *Journal of Materials Chemistry C*, 10:870–879, 2022.

[19] Hannes Raebiger, Stephan Lany, and Alex Zunger. Charge self-regulation upon changing the oxidation state of transition metals in insulators. *Nature*, 453(7196):763–766, 2008.

[20] N Dietz, I Tsveybak, W Ruderman, G Wood, and KJ Bachmann. Native defect related optical properties of $ZnGeP_2$. *Applied physics letters*, 65(22):2759–2761, 1994.

[21] Menglin Huang, Shanshan Wang, and Shiyou Chen. First-principles study on the defect physics of ternary chalcopyrite $ZnGeP_2$ through hybrid functional. *Bulletin of the American Physical Society*, 65, 2020.

[22] Jacob J. Cordell, Jie Pan, Adele C. Tamboli, Garritt J. Tucker, and Stephan Lany. Probing configurational disorder in $zngen_2$ using cluster-based monte carlo. *Phys. Rev. Materials*, 5:024604, Feb 2021.

[23] Martin T Dove, Matthew G Tucker, and David A Keen. Neutron total scattering method: simultaneous determination of long-range and short-range order in disordered materials. *European Journal of Mineralogy*, 14(2):331–348, 2002.

[24] Anna V Ceguerra, Michael P Moody, Rebecca C Powles, Timothy C Petersen, Ross KW Marceau, and Simon P Ringer. Short-range order in multicomponent materials. *Acta Crystallographica Section A: Foundations of Crystallography*, 68(5):547–560, 2012.

[25] Gilbert Newton Lewis. *Valence and the Structure of Atoms and Molecules*. 14. Chemical Catalog Company, Incorporated, 1923.

[26] William Lawrence Bragg and Evan James Williams. The effect of thermal agitation on atomic arrangement in alloys. *Proceedings of the Royal Society of London. Series A, Containing Papers of a Mathematical and Physical Character*, 145(855):699–730, 1934.

[27] William Lawrence Bragg and Evan James Williams. The effect of thermal agitation on atomic arrangement in alloys—II. *Proceedings of the Royal Society of London. Series A-Mathematical and Physical Sciences*, 151(874):540–566, 1935.

[28] Paul F Ndione, Yezhou Shi, Vladan Stevanovic, Stephan Lany, Andriy Zakutayev, Philip A Parilla, John D Perkins, Joseph J Berry, David S Ginley, and Michael F Toney. Control of the electrical properties in spinel oxides by manipulating the cation disorder. *Advanced Functional Materials*, 24(5):610–618, 2014.

[29] MD Lind and RW Grant. Structural dependence of birefringence in the chalcopyrite structure. refinement of the structural parameters of $ZnGeP_2$ and $ZnSiAs_2$. *The Journal of Chemical Physics*, 58(1):357–362, 1973.

[30] G Kimmel, Y Shimony, O Raz, and MP Dariel. Order and disorder in $ZnGeP_2$ crystals. *Materials Structure*, 6(2):149, 1999.

[31] Guoping Liu, Lei Zhang, Yucun Zhou, Luke Soule, Yangchang Mu, Wenwu Li, and Zhicong Shi. Cation-disorder zinc blende $Zn_{0.5}Ge_{0.5}P$ compound and $Zn_{0.5}Ge_{0.5}P-TiC-C$ composite as high-performance anodes for Li-ion batteries. *Journal of Materials Chemistry A*, 9(14):9124–9133, 2021.

[32] Elizabeth A Lund and Michael A Scarpulla. Modeling Cu_2ZnSnS_4(CZTS) solar cells with kesterite and stannite phase variation. In *Physics, Simulation, and Photonic Engineering of Photovoltaic Devices II*, volume 8620, page 862015. International Society for Optics and Photonics, 2013.

[33] Mirjana Dimitrievska, Federica Boero, Alexander P Litvinchuk, Simona Delsante, Gabriella Borzone, Alejandro Perez-Rodriguez, and Victor Izquierdo-Roca. Structural polymorphism in "kesterite" Cu_2ZnSnS_4: Raman spectroscopy and first-principles calculations analysis. *Inorganic Chemistry*, 56(6):3467–3474, 2017.

[34] Susan Schorr. *Crystallographic aspects of Cu2ZnSnS4 (CZTS)*. John Wiley and Sons: Chichester, 2015.

[35] SP Ramkumar, Anna Miglio, MJ Van Setten, David Waroquiers, Geoffroy Hautier, and G-M Rignanese. Insights into cation disorder and phase transitions in czts from a first-principles approach. *Physical Review Materials*, 2(8):085403, 2018.

[36] L Garbato, F Ledda, and A Rucci. Structural distortions and polymorphic behaviour in ABC_2 and AB_2C_4 tetrahedral compounds. *Progress in crystal growth and characterization*, 15(1):1–41, 1987.

[37] Rekha R Schnepf, Jacob J Cordell, M Brooks Tellekamp, Celeste L Melamed, Ann L Greenaway, Allison Mis, Geoff L Brennecka, Steven Christensen, Garritt J Tucker, Eric S Toberer, et al. Utilizing site disorder in the development of new energy-relevant semiconductors. *ACS Energy Letters*, 5(6):2027–2041, 2020.

[38] Jie Pan, Jacob J Cordell, Garritt J Tucker, Andriy Zakutayev, Adele C Tamboli, and Stephan Lany. Perfect short-range ordered alloy with line-compound-like properties in the $ZnSnN_2$:ZnO system. *npj Computational Materials*, 6(1):1–6, 2020.

[39] Paul C Quayle, Eric W Blanton, Atchara Punya, Grant T Junno, Keliang He, Lu Han, Hongping Zhao, Jie Shan, Walter RL Lambrecht, and Kathleen Kash. Charge-neutral disorder and polytypes in heterovalent wurtzite-based ternary semiconductors: The importance of the octet rule. *Physical Review B*, 91(20):205207, 2015.

[40] S. Lany, A. N. Fioretti, P. P. Zawadzki, L. T. Schelhas, E. S. Toberer, A. Zakutayev, and A. C. Tamboli. Monte carlo simulations of disorder in $ZnSnN_2$ and the effects on the electronic structure. *Physical Review Materials*, 1(3):035401, aug 2017.

[41] Foster C Nix and William Shockley. Order-disorder transformations in alloys. *Reviews of Modern Physics*, 10(1):1, 1938.

[42] Bertram Eugene Warren. *X-ray Diffraction*. Courier Corporation, 1990.

[43] Shigeru Nakatsuka and Yoshitaro Nose. Order–disorder phenomena and their effects on bandgap in $ZnSnP_2$. *The Journal of Physical Chemistry C*, 121(2):1040–1046, 2017.

[44] Mohamed H Sayed, Marco Brandl, Christine Chory, Ingo Hammer-Riedel, Jürgen Parisi, Levent Gütay, and Rainer Hock. In-situ xrd investigation of re-crystallization and selenization of CZTS nanoparticles. *Journal of Alloys and Compounds*, 686:24–29, 2016.

[45] Christopher J Bosson, Max T Birch, Douglas P Halliday, Chiu C Tang, Annette K Kleppe, and Peter D Hatton. Polymorphism in Cu_2ZnSnS_4 and new off-stoichiometric crystal structure types. *Chemistry of Materials*, 29(22):9829–9839, 2017.

[46] GC Xing, KJ Bachmann, JB Posthill, and ML Timmons. Substrate effects on the epitaxial growth of $ZnGeP_2$ thin films by open tube organometallic chemical vapor deposition. *Journal of Applied Physics*, 69(8):4286–4291, 1991.

[47] Mengdi Liu, Beijun Zhao, Baojun Chen, Zhiyu He, Shifu Zhu, Hui Liu, Hui Sun, Mingyu Sha, and Bo Feng. Research of thermodynamic properties of mid-infrared single crystal zngep2. *Materials Science in Semiconductor Processing*, 79:161–164, 2018.

[48] Jianwei Sun, Adrienn Ruzsinszky, and John P Perdew. Strongly constrained and appropriately normed semilocal density functional. *Physical Review Letters*, 115(3):036402, 2015.

[49] Jianwei Sun, Richard C Remsing, Yubo Zhang, Zhaoru Sun, Adrienn Ruzsinszky, Haowei Peng, Zenghui Yang, Arpita Paul, Umesh Waghmare, Xifan Wu, et al. Accurate first-principles structures and energies of diversely bonded systems from an efficient density functional. *Nature Chemistry*, 8(9):831–836, 2016.

[50] SK Tripathy and V Kumar. Electronic, elastic and optical properties of $ZnGeP_2$ semiconductor under hydrostatic pressures. *Materials Science and Engineering: B*, 182:52–58, 2014.

[51] Anubhav Jain, Shyue Ping Ong, Geoffroy Hautier, Wei Chen, William Davidson Richards, Stephen Dacek, Shreyas Cholia, Dan Gunter, David Skinner, Gerbrand Ceder, and Kristin a. Persson. Com-

mentary: The Materials Project: A materials genome approach to accelerating materials innovation. *APL Materials*, 1(1):011002, 2013.

[52] Agostino Zoroddu, Fabio Bernardini, Paolo Ruggerone, and Vincenzo Fiorentini. First-principles prediction of structure, energetics, formation enthalpy, elastic constants, polarization, and piezoelectric constants of AlN, GaN, and InN: Comparison of local and gradient-corrected density-functional theory. *Physical Review B*, 64(4):045208, 2001.

[53] A Vaipolin, E Osmanov, and V Prochukhan. Modifications of A(II)−B(IV)−C_2(V) compounds with the sphalerite structure. *Izv. Akad. Nauk SSSR, Neorg. Mater*, 8:947, 1972.

[54] T. Endo, H. Takizawa, and M. Shimada. New II−IV−V_2 family of periodic compounds synthesized under high pressure. In *Ceramic Engineering and Science Proceedings*, volume 13, pages 844–851. American Ceramic Society, 1992.

[55] H Pfister. Kristallstruktur von ternären verbindungen der art A(II)B(IV)C(V). *Acta Crystallographica*, 11(3):221–224, 1958.

[56] A Continenza, S Massidda, AJ Freeman, TM De Pascale, F Meloni, and M Serra. Structural and electronic properties of narrow-gap ABC_2 chalcopyrite semiconductors. *Physical Review B*, 46(16):10070, 1992.

[57] T Endo, Y Sato, Hirotsugu Takizawa, and M Shimada. High-pressure synthesis of new compounds, $ZnSiN_2$ and $ZnGeN_2$ with distorted wurtzite structure. *Journal of materials science letters*, 11(7):424–426, 1992.

[58] A Vaipolin. Specific defects of the structure of compounds $A^{2+}B^{4+}C_2^{3-}$. *Fizika Tverdogo Tela (Sankt-Petersburg)*, 15:1430–1435, 1973.

[59] G Bergerhoff, ID Brown, F Allen, et al. Crystallographic databases. *International Union of Crystallography, Chester*, 360:77–95, 1987.

[60] Timothy J Coutts, J Scott Ward, David L Young, Keith A Emery, Timothy A Gessert, and Rommel Noufi. Critical issues in the design of polycrystalline, thin-film tandem solar cells. *Progress in Photovoltaics: Research and Applications*, 11(6):359–375, 2003.

[61] Joseph Leo Shay and Jack Harry Wernick. *Ternary chalcopyrite semiconductors: growth, electronic properties, and applications: international series of monographs in the science of the solid state*, volume 7. Elsevier, 2017.

[62] Jacob J Cordell, Garritt J Tucker, Adele Tamboli, and Stephan Lany. Bandgap analysis and carrier localization in cation-disordered $ZnGeN_2$. *APL Materials*, 10(1):011112, 2022.

[63] John P Perdew, Kieron Burke, and Matthias Ernzerhof. Generalized gradient approximation made simple. *Physical Review Letters*, 77(18):3865, 1996.

[64] Vladan Stevanovic, Stephan Lany, Xiuwen Zhang, and Alex Zunger. Correcting density functional theory for accurate predictions of compound enthalpies of formation: Fitted elemental-phase reference energies. *Physical Review B*, 85:115104, 2012.

[65] G Kresse and D Joubert. From ultrasoft pseudopotentials to the projector augmented-wave method. *Physical Review B*, 59(3):1758–1775, 1999.

[66] S L Dudarev, G A Botton, S Y Savrasov, C J Humphreys, and A P Sutton. Electron-energy-loss spectra and the structural stability of nickel oxide: An LSDAU study. *Physical Review B*, 57(3):1505–1509, 1998.

[67] Stephan Lany. Band-structure calculations for the 3 d transition metal oxides in GW. *Physical Review B*, 87(8):085112, 2013.

[68] Peter Graf, Harry Sorensen, Stephen Sullivan, Ann Deml, Stephan Lany, Haowei Peng, Vladan Stevanovic, Jun Yan, and Pawel Zawadzki. Nrel materials database, 2015.

[69] B Puchala and A Van Der Ven. Thermodynamics of the Zr−O system from first-principles calculations. *Physical Review B*, 88:94108, 2013.

[70] John C Thomas and Anton Van Der Ven. Finite-temperature properties of strongly anharmonic and mechanically unstable crystal phases from first principles. *Physical Review B*, 88:214111, 2013.